DIFFUSING ACOUSTIC WAVE SPECTROSCOPY: FIELD FLUCTUATION SPECTROSCOPY WITH MULTIPLY SCATTERED ULTRASONIC WAVES

Ultrasonic Wave Transport and Spectroscopy in Complex Media I

J.H. PAGE[1] AND M.L. COWAN[2]
Department of Physics and Astronomy, University of Manitoba, Winnipeg MB R3T 2N2 Canada

D.A. WEITZ
Department of Physics and DEAS, Harvard University, Cambridge, Massachusetts 02138 U.S.A.

AND

B.A.VAN TIGGELEN
Laboratoire de Physique et Modélisation des Milieux Condensés, Maison des Magistères CNRS, 25 Avenue des Martyrs, B.P. 166, 38042 Grenoble Cedex 9, France

Abstract. Diffusing Acoustic Wave Spectroscopy (DAWS) is a powerful technique in field fluctuation spectroscopy for investigating the dynamics of strongly scattering media and studying mesoscopic wave phenomena. The principles underlying DAWS are described and illustrated with measurements of the particle velocity fluctuations in fluidized suspensions. Two examples of the potential of DAWS for elucidating mesoscopic wave physics are presented: understanding the phase statistics of temporally fluctuating multiply scattered fields, and investigating the breakdown of the Siegert relation for multiply scattered waves when correlations exist in the scattering medium.

1. Introduction

The role that acoustic waves, and ultrasonic waves in particular, are playing in understanding the rich diversity of wave phenomena in complex media [3, 4, 5, 6] is becoming increasing appreciated. In large part, this role reflects the fact that ultrasonic techniques measure the wave field directly, without

the need for complicated interferometry, and are normally easier to perform with pulses than with continuous waves (cw). The advantage of the first is that it gives direct experimental access to the wave function and/or Green's function, while the second allows the dynamics of the wave fields to be explored, as well as the time-of-flight distribution or path-length dependence of multiply scattered waves. Furthermore, scattering contrast is governed by differences in both density and velocity, offering versatile control of the scattering strength. Thus, experiments with acoustic and elastic waves can make important contributions to both fundamental studies and practical applications of wave scattering in complex media, and are complementary to optical and microwave methods for investigating these phenomena.

This is the first of two papers that summarize recent progress in using ultrasonic waves to explore two different aspects of wave transport and spectroscopy in strongly scattering media. In this paper we focus on random systems in which the scatterers are moving, and describe a technique in field fluctuation spectroscopy, called Diffusing Acoustic Wave Spectroscopy (DAWS), that uses multiply scattered waves to measure their dynamics [7, 8, 9, 10]. We review the application of this technique to investigating the dynamics of particles in fluidized suspensions, where a detailed understanding of the complex particulate flows has remained elusive, despite the fact that the dynamics are mediated by one of the simplest many-body interactions, the hydrodynamic interactions between particles in a liquid. We also show how DAWS provides an opportunity to study fundamental properties of multiply scattered waves through the measurement of phase and amplitude fluctuations. In the second paper, we turn to ordered systems and examine ultrasonic wave propagation and tunnelling in three-dimensional phononic crystals, where the character of waves is strongly modified by the existence of band gaps and anisotropy of the wave speeds.

The organization of this paper is as follows. In section 2, we present measurements and theory of the pulsed DAWS field autocorrelation function, highlighting the dynamic quantities that can be measured in fluidized suspensions of particles. Section 3 deals with measurements of the phase and amplitude of multiply scattered waves, focusing on the phase statistics of time-varying fields and what can be learned from the comparison of field and intensity correlation functions. The paper ends with some concluding remarks and prospects for future work.

2. The Pulsed DAWS Field Autocorrelation Function and Scatterer Dynamics

When the scatterers in a multiple scattering material move, the speckle pattern fluctuates, reflecting the changes that occur in the interference of

waves travelling different scattering paths through the sample. In Diffusing Acoustic Wave Spectroscopy, these fluctuations of the multiply scattered wave field $\psi(T)$ are measured in one (or more) speckle spots and analyzed to provide a sensitive technique for probing the dynamics of the scatterers. The most direct way of determining the movement of the scatterers is through the autocorrelation function of the scattered acoustic field,

$$g_1(\tau) = \frac{\int \psi(T)\ \psi^*(T+\tau)\, dT}{\int |\psi(T)|^2 dT}. \tag{1}$$

The relationship between $g_1(\tau)$ and the scatterers' dynamics can be illustrated qualitatively by noting that $g_1(\tau)$ decays to approximately $1/2$ when the total rms change in phase of the scattered field due to the scatterers' motion is about a radian. Here we use T to denote the time scale on which the fluctuations in the scattered field are measured, as distinct from the propagation time t of acoustic waves in the sample ($t \ll T$). To facilitate the calculation of $g_1(\tau)$ when the waves are multiply scattered, and hence link the phase change directly to the dynamics of the scatterers, we model the propagation of sound though the material using the diffusion approximation. Thus, we take advantage of the simple physical picture of wave transport in a multiple scattering medium as a random walk process along paths characterized by a step length equal to the transport mean free path l^*, which is related to the energy velocity v_e and the diffusion coefficient D by $D = v_e l^*/3$. In this paper we will illustrate the technique by reviewing the application of DAWS to investigating the motion of particles in a fluidized bed, where all the scatterers are moving in locally correlated flow patterns that evolve rapidly in time. In this case, DAWS measures the relative mean square displacement of the scattering particles that are separated, on average, by a distance equal to the transport mean free path. The method can obviously be generalized to many other scenarios, such as those where only a fraction of the scatters may move or where the type of motion or system dynamics is entirely different.

Pulsed DAWS, in which the incident signal is a short pulse or tone burst, provides an important advantage over a cw (continuous wave) approach in that it allows the field fluctuations to be measured for multiple scattering paths of fixed length $s = (n+1)l^*$, where n is the number of steps. If we isolate one such path, the phase change resulting from the motion of all the scatterers p along the path is

$$\Delta\phi^{(n)}(\tau) \quad = \quad \sum_{p=0}^{n} \Delta\phi_p(\tau)$$

$$= \sum_{p=0}^{n} \left[\vec{k}_p \cdot \left(\Delta \vec{r}_{p+1}(\tau) - \Delta \vec{r}_p(\tau) \right) \right]$$
$$\simeq \sum_{p=1}^{n-1} \vec{k}_p \cdot \Delta \vec{r}_{rel,p}(\tau, l^*), \quad (2)$$

where we have neglected (for the time being) the phase change due to motion of the first and last scatterer relative to the source and detector, as this is a small contribution for large n. Here $\vec{k}_p$ is the wave vector of the wave scattered from the p^{th} to the $(p+1)^{th}$ particle, and $\Delta \vec{r}_{rel,p}(\tau) = \Delta \vec{r}_{p+1}(\tau) - \Delta \vec{r}_p(\tau)$ is their relative displacement during the time interval τ. By averaging over all paths with n steps, assuming that the successive phase shifts $\Delta\phi_p(\tau)$ are uncorrelated, and using a cumulant expansion, the pulsed field correlation function can be written in terms of the variance of the phase change per scattering event p as

$$g_1(\tau) = \left\langle \exp\left[-i\Delta\phi^{(n)}(\tau) \right] \right\rangle \simeq \left\langle \exp\left[-i\Delta\phi_p(\tau) \right] \right\rangle^n$$
$$\simeq \exp\left[-\left\langle \Delta\phi_p^2(\tau) \right\rangle n/2 \right] \quad (3)$$

Hence $g_1(\tau)$ can be written in terms of the relative mean square displacement of the scatterers using Eq. (2), from which we obtain $\left\langle \Delta\phi_p^2(\tau) \right\rangle = \left\langle (\vec{k}_p \cdot \Delta \vec{r}_{rel,p})^2 \right\rangle = \left\langle (k_p\ \Delta r_{rel,p}(\theta_p)\ \cos\theta_p)^2 \right\rangle$, where θ_p is the angle between $\Delta \vec{r}_{rel,p}$ and $\vec{k}_p$. In particular, when there are no correlations between the directions of $\Delta \vec{r}_{rel,p}$ and $\vec{k}_p$, the phase change can be written as $\left\langle \Delta\phi_p^2(\tau) \right\rangle = k^2 \left\langle \Delta r_{rel}^2 \right\rangle / 3$. Thus, the autocorrelation function takes on the simple form:

$$g_1(\tau) \approx \exp\left[-\frac{nk^2}{6} \left\langle \Delta r_{rel}^2(\tau, l^*) \right\rangle \right]. \quad (4)$$

This equation shows clearly that the decay of $g_1(\tau)$ is governed by the relative mean square displacement $\left\langle \Delta r_{rel}^2(\tau, l^*) \right\rangle$ of particles that are separated by the average step length l^* of the diffusing sound's random walk paths through the sample.

For fluidized suspensions where the spatial correlations decay rapidly, Eq. (4) is a very good approximation for $g_1(\tau)$. However, for other types of flows, it may be necessary to account for correlations in θ_p. For example, in uniform shear flow, $\left\langle \Delta\phi_p^2(\tau) \right\rangle = 0.6k^2 \left\langle \Delta r_{rel}^2 \right\rangle / 3$, while in pure rotational flow $\left\langle \Delta\phi_p^2(\tau) \right\rangle = 0$ [10]. In general, these correlations can be accounted for formally by expressing $g_1(\tau)$ in terms of the average local strain as

$$g_1(\tau) \approx \exp\left[-\frac{nk^2 l^{*2}}{6} \bar{\varepsilon}^2(\tau, l^*) \right], \quad (5)$$

where

$$\bar{\varepsilon}^2 \equiv \tfrac{2}{5}\left[\left\langle\left(\sum \varepsilon_{ii}\right)^2\right\rangle + 2\sum_{i,j}\left\langle\varepsilon_{ij}^2\right\rangle\right], \tag{6}$$

$\varepsilon_{i,j}$ is the strain tensor

$$\varepsilon_{ij}(\tau) = \tfrac{1}{2}\left(\frac{\partial u_i(\tau)}{\partial r_j} + \frac{\partial u_j(\tau)}{\partial r_i}\right), \tag{7}$$

and $u_i(\tau)$ are the components of $\Delta\vec{r}(\tau)$ [10, 11, 12]. For uncorrelated motion, $\bar{\varepsilon}^2 = \left\langle \Delta r_{rel}^2 \right\rangle / l^*$, and Eq. (5) reduces to Eq. (4) as expected.

To illustrate the application of pulsed DAWS to investigating the dynamics of particulate suspensions, experiments were performed on a fluidized bed containing 0.88-mm-diameter glass beads in a liquid mixture of water and glycerol. By flowing the liquid vertically upward to counterbalance gravitational sedimentation, stable suspensions could be achieved over a wide range of particle volume fractions ϕ by varying the flow velocity V_f. Even under quiescent conditions at low flow velocities, the fluctuations in the particle velocities are remarkably large, and DAWS offers a novel approach for addressing some of the outstanding scientific challenges in understanding their complex behaviour. As discussed elsewhere in more detail [7, 13], some of the important questions that can be investigated using DAWS include how the dynamics of the particles are influenced by volume fraction, system size and Reynolds number, which measures the relative importance of viscous and inertial effects in the hydrodynamic interactions between the particles.

The majority of our experiments [10] to investigate these effects have been performed by sending a train of short ultrasonic pulses, with a central carrier frequency of typically 2 MHz, towards the sample and measuring the scattered field at a particular transit time t_s after each pulse has entered the sample. The experiments described here were performed in transmission mode, with the fluidized bed immersed in a large water tank, using a small hydrophone to detect the scattered field within a single speckle spot on the far side of the sample from the incident beam. In this pulsed realization of DAWS, the pulse repetition frequency sets the rate at which the field fluctuations are measured, and the sampling time t_s sets the average path length of diffusing sound in the sample and hence the number of scattering events n since $n \approx s/l^* - 1 \approx s/l^* = v_e\, t_s/l^*$. From digitized records of temporal field fluctuations at a particular value of n, acquired using a digital oscilloscope PC card, the field correlation function was calculated numerically using fast Fourier transforms and the correlation theorem, which allows the correlation function to be efficiently determined. An example of pulsed DAWS field autocorrelation functions measured for different values of n is

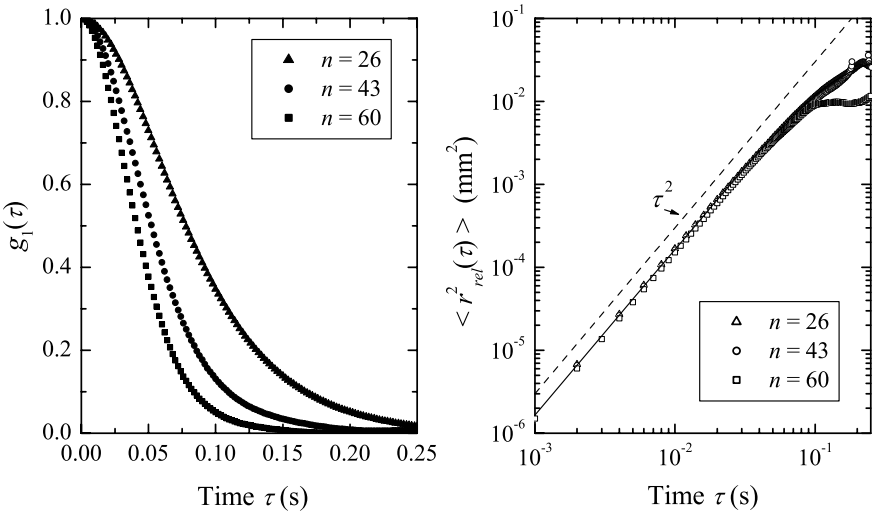

Figure 1. Field autocorrelation functions for several values of n in pulsed DAWS (left) and corresponding values of the mean square relative displacements as a function of time for particles in a fluidized bed (right).

shown in Fig. 1. As t_s and hence n increases, the fluctuations become more rapid due to accumulation of larger total phase changes along the longer paths involved, and the correlation function decays more quickly. Making use of independent measurements of the transport mean free path l^*, the energy velocity v_e and the wave vector $k = \omega/v_p$ of diffusing acoustic waves in the suspension [14, 15, 16, 17, 18, 10], Eq. (4) can be inverted to determine the relative mean square displacements of the particles, shown on the right side of Fig. 1. Despite the large differences in the correlation functions measured at the different sampling times, essentially identical values of the relative mean free paths are found, indicating that the dependence on path length in Eq. (4) correctly describes the data for this range of values of n. It is also worth noting that measurements at large values of n (longer t_s) give better sensitivity to small displacements at early times (down to nearly a micron, or $\approx \lambda/500$ for these data), because of the more rapid decay of the correlation function noted above. By contrast, smaller n (shorter t_s) can be used to increase the sensitivity to larger displacements of the particles, as the correlation function can be measured for longer times before it reaches the noise level; this is evident in Fig. 1 where it can be seen that the measurements for $n = 60$ saturate at $\left\langle \Delta r^2_{rel}(\tau) \right\rangle < 0.01$, while the maximum measurable value of $\left\langle \Delta r^2_{rel}(\tau) \right\rangle$ for $n = 26$ is a factor of 3-4 times bigger.

Figure 1 also shows that $\langle \Delta r_{rel}^2(\tau) \rangle$ varies quadratically with time, at least for $\tau < 0.1$ s, indicating that the particles follow ballistic trajectories for short times. Eventually, these ballistic trajectories become altered by interactions with neighbouring particles in the suspension, and the rate at which $\langle \Delta r_{rel}^2(\tau) \rangle$ increases slows down. We represent this behaviour with the empirical expression

$$\langle \Delta r_{rel}^2(\tau) \rangle = \frac{\langle \Delta V_{rel}^2 \rangle \tau^2}{1 + (\tau/\tau_{cl})^2} \tag{8}$$

where $\langle \Delta V_{rel}^2 \rangle$ is the variance in the relative velocities of the particles and τ_{cl} is the local crossover time, or the average time interval during which the local relative motion of the particles is not impeded by inter-particle "collisions". The solid curve in Fig. 1 shows a fit of this expression to the data, and gives an excellent description of the time dependence over four orders of magnitude in $\langle \Delta r_{rel}^2(\tau) \rangle$ and more than two orders of magnitude in τ. From this fit, an accurate measurement of the rms relative velocity fluctuations of the particles $\Delta V_{rel} = \sqrt{\langle \Delta V_{rel}^2 \rangle}$ is obtained, as well as a good indication of the average change in particle separation $\Delta d_{sep} = \Delta V_{rel} \tau_{cl}$ before interactions modify the particle trajectories.

The path length dependence of the measurements in pulsed DAWS is examined in more detail in Fig. 2, where data at shorter path lengths are also included. In order to correctly analyze data for short paths (small n), it is necessary to consider the contributions to g_1 due to the motion of the first and last scatterer relative to the source and detector, respectively. As shown by Cowan *et al.* [10], this can be accomplished by adding a correction term to $\langle \Delta r_{rel}^2(\tau, l^*) \rangle$ in Eq. (4) given by $[\langle \Delta r_{rel}^2(\tau, R) \rangle - \langle \Delta r_{rel}^2(\tau, l^*) \rangle]/n$. Here R is the linear distance between the first and last scatterer. This correction term is zero if the motion of the scatterers is uncorrelated for $R \geq l^*$, but its magnitude is otherwise of order $1/n$. For fluidized suspensions, where there are significant local correlations in the velocities of the particles, this term may not be negligible if the path length is short enough. The experimental data indicated by the symbols in Fig. 2 show that this is indeed the case. In this figure, we plot ΔV_{rel} determined from Eq. (4) without this correction, divided by an extrapolation of ΔV_{rel} as $n \to \infty$. For $n < 20$, this ratio becomes significantly larger than unity, showing that appreciable errors in the measurement of ΔV_{rel} will result if the correction is not taken into account. Fig. 2 also compares a fit of the correction term to the data for $\phi = 0.50$, normalized in the same way, which is shown by the dashed curve. In this fit, there is one unknown: $\langle \Delta V_{rel}^2(R) \rangle = \langle \Delta r_{rel}^2(R) \rangle / \tau^2$. It is clear from Fig. 2 that the correction term does indeed give a satisfactory fit to the data; furthermore it yields a value of $\Delta V_{rel}(R)$ that is physically reasonable,

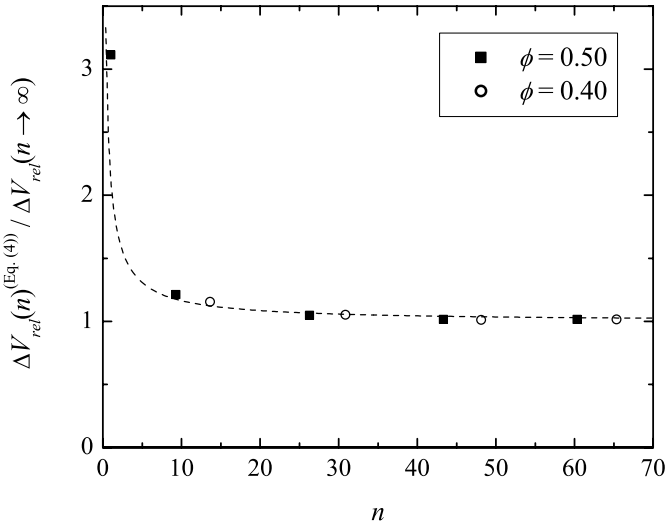

Figure 2. Values of ΔV_{rel} as a function of the number of scattering events n determined from Eq. (4), without accounting from the motion of the first and last scatterer with respect to the source and detector. The data are normalized by the limiting values of ΔV_{rel} at large n, and compared with a fit to the correction term described in the text (dashed curve).

lying between the minimum possible value at $R = L$, where L is the sample thickness, and the maximum possible value at $R = \xi$, where ξ is the velocity correlation length (see below). These results show that this correction term can be used to make measurements for short paths and hence extend the range of paths lengths over which data can be collected. They also show that the simple expression for $g_1(\tau)$ given by Eq. (4), neglecting the motion of the first and last scatterers relative to the source and detector, accurately accounts for the path length dependence in the correlation function for n greater than about 20.

Most of our DAWS measurements have been performed using quasi-plane wave input pulses generated in the far field of planar immersion transducers. To improve signal to noise, a focusing transducer can be used to focus the input pulse on the sample face, producing a quasi-point source. The advantage of a point source is that there is more signal, since all of the input energy is focused down on a small spot, instead of being spread out in a quasi-plane wave. Since extensive signal averaging cannot be used to measure time varying fields, other ways of optimizing signal to noise can be especially important in DAWS. While in principle, the source geometry

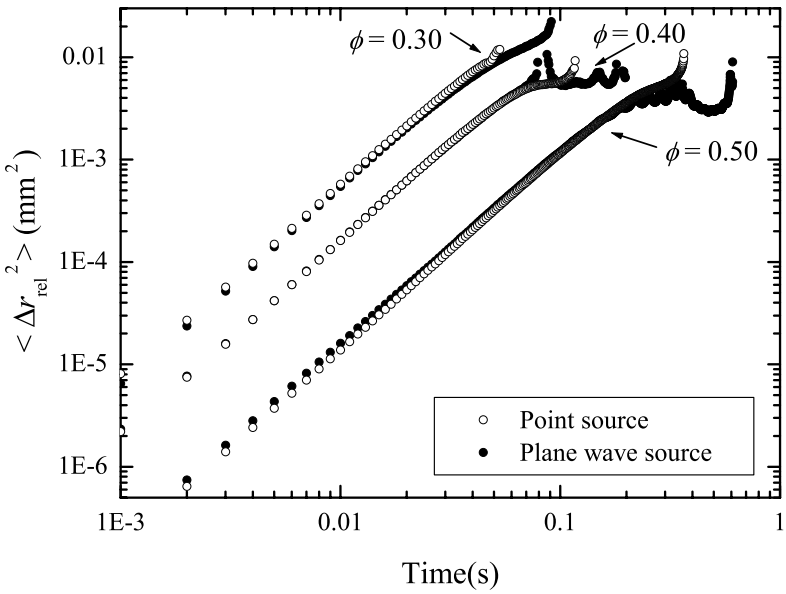

Figure 3. Comparison of DAWS experiments performed with a point source (open symbols) and plane wave source (closed symbols).

should not matter, as what counts is only the the average length of the scattering paths that are being measured, it is still important to check that this holds in practice. Fig. 3 shows the results of such a test, where data for $\langle \Delta r_{rel}^2(\tau) \rangle$ using a point source are compared with data obtained with a planar source for three volume fractions ϕ of scatterers. The very good agreement between the data taken with these two different input geometries demonstrates that focussing transducers can indeed be used reliably to increase the single-to-noise ratio in DAWS, and provides a useful check of the robustness of the DAWS technique itself.

As emphasized above, DAWS measures the relative motion of the scatterers $\Delta V_{rel}(R)$ on a length scale determined by the transport mean free path of the ultrasound, l^*. By changing the ultrasonic frequency, l^* can be varied, since the strength of the scattering is strongly frequency dependent near the edge of the strong scattering regime where the wavelength becomes comparable with the size of the scatterers [15, 16, 18]. Thus, the spatial correlations in the particle velocities can be investigated over a range of length scales, down to distances comparable with the average nearest neighbour separation of the particles [7, 10]. In particular, the variance in the local

relative velocity of the particles can be written

$$\begin{aligned}\left\langle \Delta V_{rel}^2\left(l^*\right)\right\rangle &= \left\langle \left[\Delta\vec{V}\left(\vec{r}+l^*\right)-\Delta\vec{V}\left(\vec{r}\right)\right]^2\right\rangle \\ &= 2\left\langle \Delta V^2\right\rangle - 2\left\langle \Delta\vec{V}\left(\vec{r}+l^*\right)\cdot\Delta\vec{V}\left(\vec{r}\right)\right\rangle \\ &= 2\,V_{rms}^2\left(1-\exp\left[-l^*/\xi\right]\right), \end{aligned} \tag{9}$$

showing explicitly how the relative velocity variance is related to the absolute particle velocity variance V_{rms}^2 and the velocity correlation function. The last line of this equation assumes that the velocity correlations decrease exponentially as the distance between the particles increases, with a characteristic decay length given be the velocity correlation length ξ. Since V_{rms} can be measured using Dynamic Sound Scattering (DSS) in the single scattering regime at low frequencies [7, 13], the instantaneous velocity correlation length can be measured from the dependence of the relative velocity fluctuations on l^*. Experimental data over a wide range of volume fractions from 0.08 to 0.50 are shown in Fig. 4, where the relative velocity is normalized by the asymptotic value at large distances $\sqrt{2}V_{rms}$, and the measurement length scale l^* is normalized by the correlation length ξ. Fig. 4 shows that for small inter-particle separations, the relative velocity increases as the square root of distance, but levels off as the correlation length is approached. The predictions of Eq. (9) are represented by the solid curve and are in very good agreement with the data, confirming that the velocity correlation function decreases exponentially with distance and indicating the velocity correlation length of the particles can be reliably measured using this technique.

We end this section with a couple of examples of typical data, taken as part of an extensive investigation of the velocity fluctuations in fluidized suspensions [13]. For these data, the particle Reynolds number Re_p is 0.9, a value at which we find very similar behaviour to that in creeping flow conditions at much lower Re_p, even though it is close to the range where inertial effects are expected to become important. Fig. 5(a) shows the volume fraction dependence of the relative velocity fluctuations at a distance given by the nearest neighbour particle separation, the shortest distance in the suspension over which the local relative velocity can be defined. In this figure, the velocity is normalized by the average fluid velocity V_f. Data from three rectangular cells with different thicknesses L_z are included, the other dimensions of the cells being larger and constant at 1030 and 407 bead radii a. The relative velocity is remarkably large even at these short length scales, being similar in magnitude to V_f, and increases with volume fraction ϕ as $\phi^{1/3}$ up to $\phi \sim 0.4$. At the highest ϕ, the relative velocity drops as the particles move more in step with each other. Note that throughout

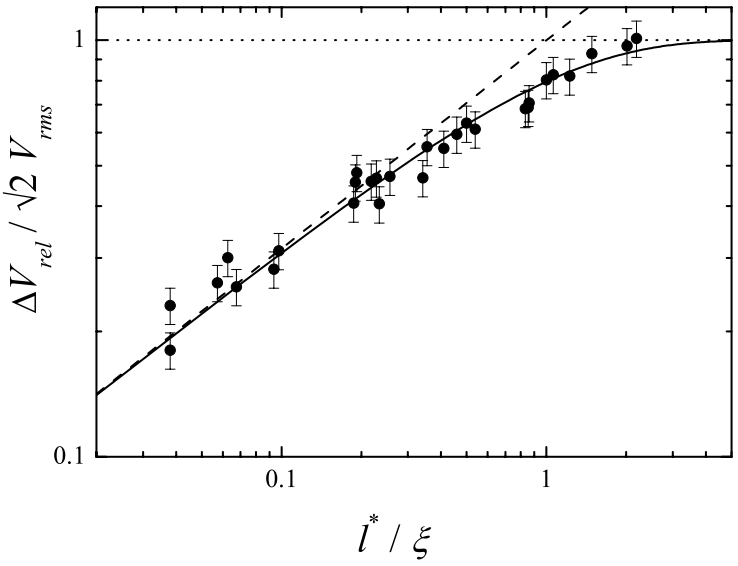

Figure 4. Scaling plot showing the length scale dependence of ΔV_{rel}. Here $\Delta V_{rel}(l^*)$ is normalized by the value reached at large distances where the motion is uncorrelated ($\sqrt{2}V_{rms}$), and the average separation between the particles at each measurement of ΔV_{rel} is normalized by the measured correlation length ξ. The solid curve represents the predictions of Eq. (9), and the dashed line represents the $\sqrt{l^*/\xi}$ dependence seen at short length scales.

this range of volume fractions, the local relative velocity is unaffected by the thickness of the cell, even when the shortest distance between the walls is as small as 10 particle diameters. By contrast, the velocity correlation length, shown in Fig. 5(b), shows a larger variation with volume fraction and decreases significantly as the thickness of the cell is reduced. The volume fraction dependence is similar for the different cells, despite the fact that the magnitude of the correlation length may be either substantially larger or smaller than the smallest cell dimension. For $\phi \lesssim 0.2$, the volume fraction dependence is consistent with $\phi^{-1/3}$ behaviour expected if the number of particles in the correlation volume is independent of volume fraction and is in agreement with the extrapolation of measurements using particle imaging velocimetry at low ϕ and Re_p [19]. However, at higher ϕ the correlation length increases quite rapidly, approximately linearly in ϕ, indicating that the number of particles in the correlation volume grows rapidly as ϕ^4. The fact that the thickness of the cells influences the magnitude of the correlation length indicates that cell walls play a major role

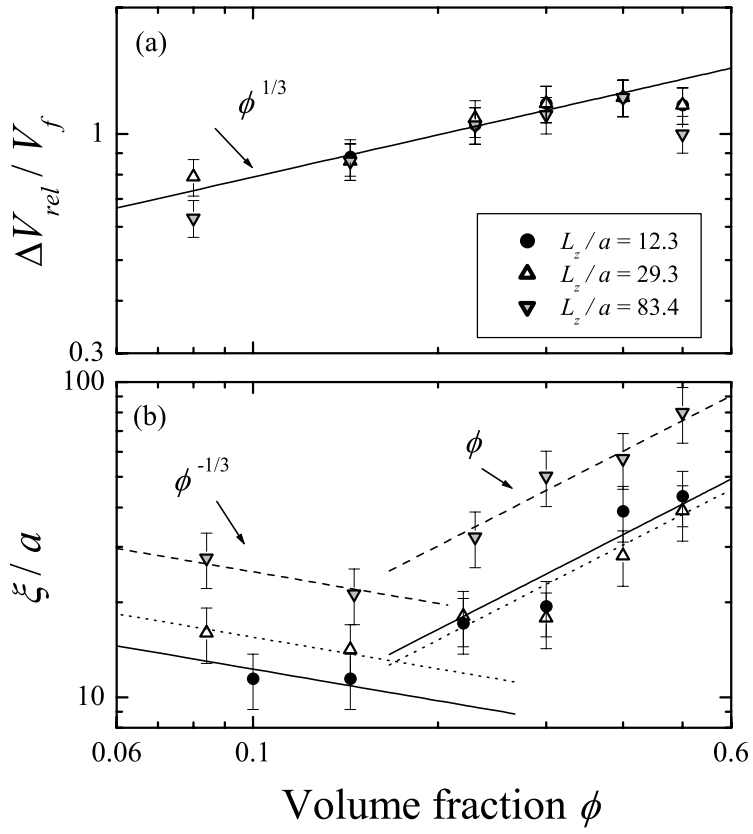

Figure 5. (a) The root mean square relative velocity at the nearest-neighbour particle separation, normalized by the fluid velocity V_f, as a function of volume fraction. Data for three sample thicknesses are shown. The solid line shows the $\phi^{1/3}$ dependence that is consistent with the data up to $\phi \sim 0.4$. (b) The volume fraction dependence of the instantaneous velocity correlation length, normalized by the particle radius, for the same three values of sample thickness. The data are consistent with a $\phi^{-1/3}$ dependence at low ϕ and a linear dependence at high ϕ, as indicated by the solid, dotted and dashed lines which represent fits to the data for the three thicknesses.

in determining the spatial extent of the velocity correlations, at least in small cells. These data suggest the following simple physical picture: the magnitude of the velocity fluctuations in fluidized suspensions may be set initially at the local level by the relative motion of neighbouring particles in the suspension, the relative motion then growing with the square root of distance until the fluctuations are cut off at the correlation length by cell walls or other screening effects [20, 21, 22]. However, the development of

a microscopic model of the particle dynamics observed in our experiments remains an intriguing theoretical challenge.

3. Phase and Amplitude Fluctuations of Multiply Scattered Waves

In addition to being a powerful technique for probing the dynamic behaviour of multiple scattering systems, DAWS provides an almost unique opportunity to investigate fundamental properties of multiply scattered waves. This opportunity arises naturally from the ability of ultrasonic techniques to directly access the multiply scattered wave field, as opposed to the scattered intensity, and the relative ease with which this can be accomplished compared to optical techniques . Thus, the temporal evolution of both the phase and amplitude of the wave field can be measured independently, and their statistical behaviour analyzed. Furthermore, using a pulsed technique, this information can be obtained as a function of the path length of the multiply scattering waves in the sample, potentially adding additional insight into the nature of the wave fields. Here we address the following question: what can we learn using DAWS, both about wave physics and the dynamic properties of complex media, from the amplitude and phase fluctuations of multiply scattered ultrasonic waves?

The measurement of the phase and amplitude of the scattered field was performed as follows (see Fig. 6). Again we use moving spherical glass particles in a fluidized bed as an archetypical dynamic system to illustrate the method. In order to maximize the rate at which the data could be recorded, a short segment of the entire transmitted waveform (top panel of Fig. 6) was recorded for each repetition of the input pulse, each segment being about 4.5 periods long. The segments were centered around a fixed sampling time $t_s = 18$ μs after the input pulse arrived at the sample, each time window corresponding to an average of 34 ± 2 scattering events. Typical data for the scattered field segments, recorded at time intervals separated by 150 repetitions of the input pulse (pulse repetition frequency = 500 Hz), are shown in the left column of the bottom panel of Fig. 6. We used a simple numerical technique to determine the phase and amplitude, in which the digitized field data are first multiplied by a sine and cosine wave at the central frequency of the pulse and then low-pass filtered to extract the dc components $S(t)$ and $C(t)$; the amplitude and phase are then given by $A(t) = 2\sqrt{S^2(t) + C^2(t)}$ and $\varphi(t) = \tan^{-1}[-S(t)/C(t)]$. The frames in the middle and right columns of the bottom panel illustrate snapshots of the amplitude and wrapped phase [$-\pi : \pi$] for different positions of the scatterers after they have moved during 0.75 s intervals. To measure the amplitude and phase fluctuations with good statistical accuracy, 10 sets of 8300 consecutive pulses were recorded.

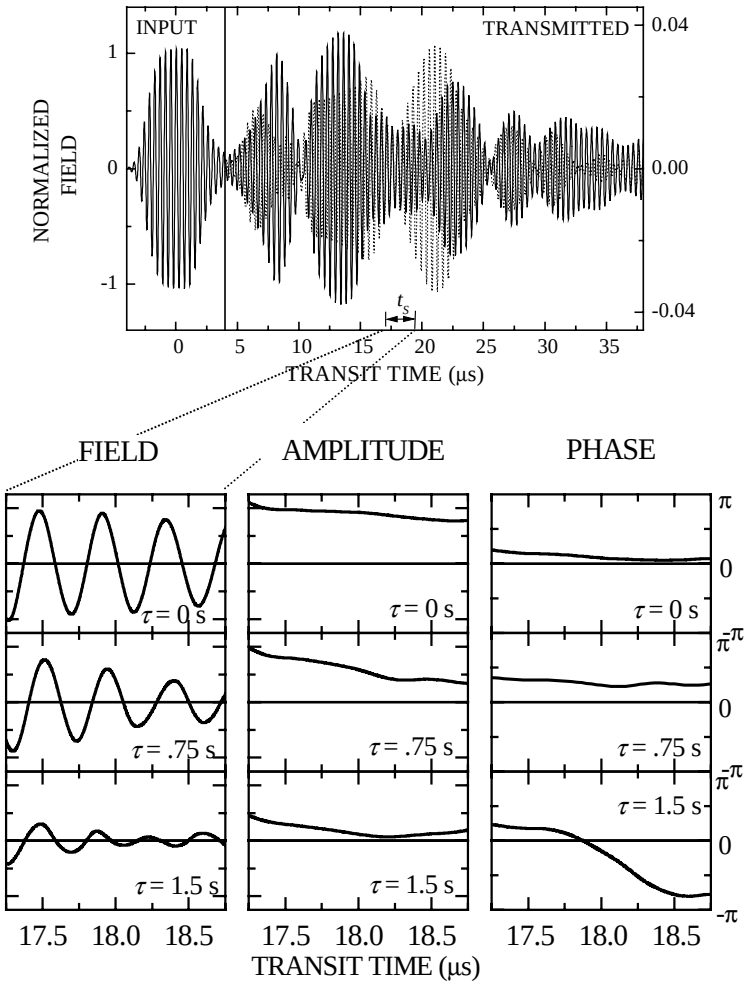

Figure 6. Top panel: The input and transmitted pulses in a typical transmission DAWS experiment. Two transmitted pulses, measured after a sufficiently long time interval that the field has evolved considerably, are shown by the solid and dotted traces. Bottom panel: Three snapshots of the scattered wave field, amplitude and phase (left, middle and right columns) in a 1.5 μs long window after the scatterers have moved during time intervals of $\tau = 0.75$ s.

An example of the evolution of the measured amplitude and phase fluctuations at three different sampling times is plotted in Fig. 7. The three times correspond to times which are 0.15, 0.5, and 0.85 of the way across the segment windows shown in Fig. 6. These sampling times are far enough away from each other that the amplitudes and phases are not the same;

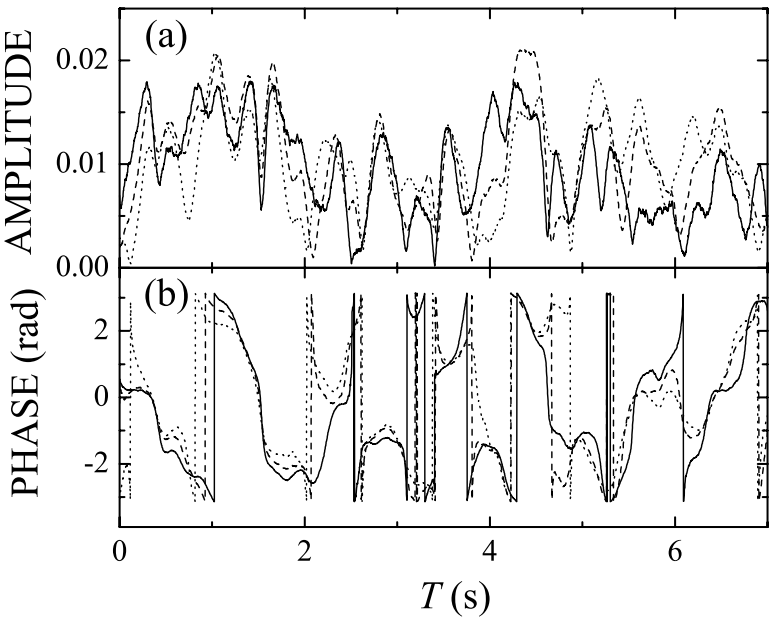

Figure 7. Evolution of (a) the amplitude and (b) the wrapped phase at three different sampling times, corresponding to times near the beginning, at the middle and near the end of the segment windows shown in Fig. 6. The amplitude is expressed in arbitrary units corresponding to the voltage measured on the digital oscilloscope.

however, they are still very strongly correlated. The amplitude gets extremely close to zero several times in the 7 seconds shown, which is typical for this data set; on average this occurs about once every 2 seconds. The variations for the same three sampling times are shown in Fig. 7(b). The behavior of the wrapped phase at the three sampling times is very similar, except for differences during the rapid variations of π in the phase that occur in the dark speckles when the amplitude is close to zero.

The first-order statistics of the scattered intensity ($I(T) \propto |A(T)|^2$) and phase ($\varphi(T)$) are shown in Fig. 8. The probability density function for the intensity (Fig. 8(a)) shows the usual negative exponential form characteristic of Rayleigh statistics of uncorrelated speckles, for which $P(I) = (1/I_{ave}) \exp(-I/I_{ave})$. The solid curve in Fig. 8(a) is a fit of this distribution to the data, and confirms that the standard deviation is equal to the mean, as expected [23]. Figure Fig. 8(b) shows that the corresponding phase distribution function is flat between -π and +π, i.e. the phases are distributed randomly with $P(\varphi) = 1/(2\pi)$. Together, these results indi-

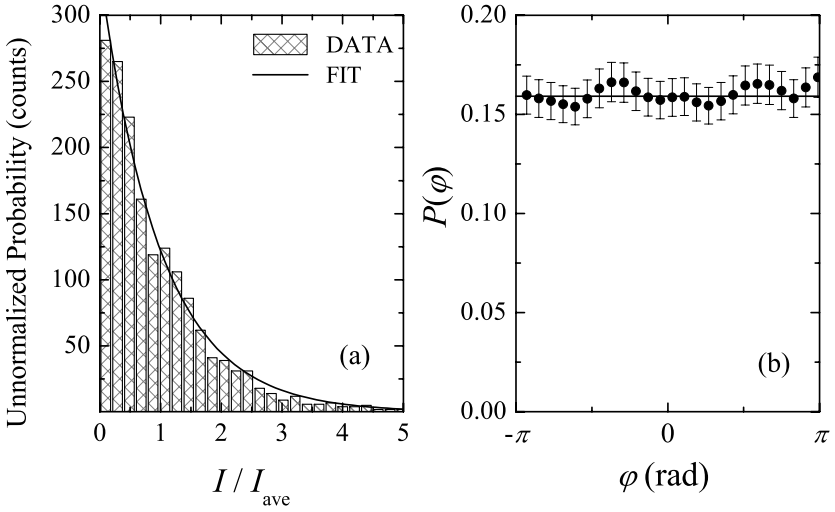

Figure 8. Probability distributions of (a) the intensity and (b) the wrapped phase of multiply scattered acoustic waves in fluidized suspensions.

cate that the multiply scattered wave field is a complex Gaussian random variable, despite the correlations in the motion of the scatterers discussed in the previous section.

3.1. PHASE INFORMATION: THE WRAPPED PHASE DIFFERENCE PROBABILITY DISTRIBUTION

To gain more insight into the phase statistics of multiply scattered waves and to see how information on the scatterer dynamics can be uncovered, we examine the phase difference $\Delta\varphi(\tau) = \varphi(T+\tau) - \varphi(T)$. Because of the random character of the wave field, we are forced to take a statistical approach. The statistics of the phase difference can be obtained from the joint probability distribution $P(\psi_T, \psi_{T'})$ of the fields at times T and $T' = T + \tau$. For a complex Gaussian process, $P(\psi_T, \psi_{T'})$ can be written [23, 24]

$$P\left(\psi_T, \psi_{T'}\right) = \frac{1}{\pi^2 \det \mathbf{C}} \exp\left(- \sum_{i,j=T,T'} \psi_i^* C_{ij}^{-1} \psi_j \right), \tag{10}$$

where $C_{ij} = \langle \psi_i \psi_j^* \rangle$ is the covariance matrix. We normalize the fields so that $\langle \psi_i \psi_i^* \rangle = \langle |\psi(T)|^2 \rangle = 1$ and $\langle \psi_i \psi_j^* \rangle = g_1(\tau)$, the field autocorrelation function. Eq. (10) for $P(\psi_T, \psi_{T'})$ can then be rewritten in terms of the

amplitude and phase to give

$$P\left(A_T, A_{T'}, \varphi_T, \varphi_{T'}\right) = \frac{A_T A_{T'}}{\pi^2\left(1-g_1^2\right)} \times \exp\left\{-\frac{A_T^2 + A_{T'}^2 - 2g_1 A_T A_{T'}\cos\left(\varphi_T - \varphi_{T'}\right)}{1-g_1^2}\right\}. \tag{11}$$

The wrapped phase difference probability distribution can then be obtained from Eq. (11) by integrating out the dependence on A_T, A'_T and φ'_T at constant $\Delta\varphi$, giving

$$P\left(\Delta\varphi\right) = \frac{2\pi - |\Delta\varphi|}{4\pi^2}\left[\frac{1-g_1^2}{1-g_1^2\cos^2\left(\Delta\varphi\right)}\right] \times \left[1 + \frac{g_1\cos\left(\Delta\varphi\right)\arccos\left\{-g_1\cos\left(\Delta\varphi\right)\right\}}{\sqrt{1-g_1^2\cos^2\left(\Delta\varphi\right)}}\right]. \tag{12}$$

Eq. (12) shows that the wrapped phase difference probability distribution contains information on the dynamics of the scatterers through its dependence on $g_1(\tau)$. At short times and small $\Delta\varphi$, $P(\Delta\varphi)$ can be written as a simple algebraic law

$$P\left(\Delta\varphi\right) \cong \frac{\frac{1}{2}\left\langle\Delta\phi^2\left(\tau\right)\right\rangle}{\left[\left\langle\Delta\phi^2\left(\tau\right)\right\rangle + \Delta\varphi^2\right]^{3/2}}, \tag{13}$$

whose width $\langle\Delta\phi^2\left(\tau\right)\rangle \simeq n\langle\Delta\phi_p^2\left(\tau\right)\rangle$ is the variance of the change in phase for all paths containing n scattering events (c.f. Eq. (3)) and is related to the relative motion of the scatterers through Eq. (4). This equation, which is equivalent to the probability distribution for the phase derivative with time $P(d\varphi/d\tau)$, has the same form as the distribution for the phase derivative with frequency investigated previously with microwaves [25, 24]. At long times, the phase difference probability distribution approaches a triangular function

$$P\left(\Delta\phi\right) = \frac{2\pi - |\Delta\phi|}{4\pi^2}, \tag{14}$$

reflecting the complete lack of correlations in the phase difference as $\tau \to \infty$ and the underlying phase distribution is flat in $[-\pi : \pi]$.

These theoretical predictions for the phase derivative probability distribution are compared with experiment in Fig. 9, where our measurements of $P(\Delta\varphi)$ at two different times τ (representative of the behaviour at small and large τ) are plotted along with fits of Eq. (12) to the data. At the relatively short time of $\tau = 20$ ms, the central part of the distribution

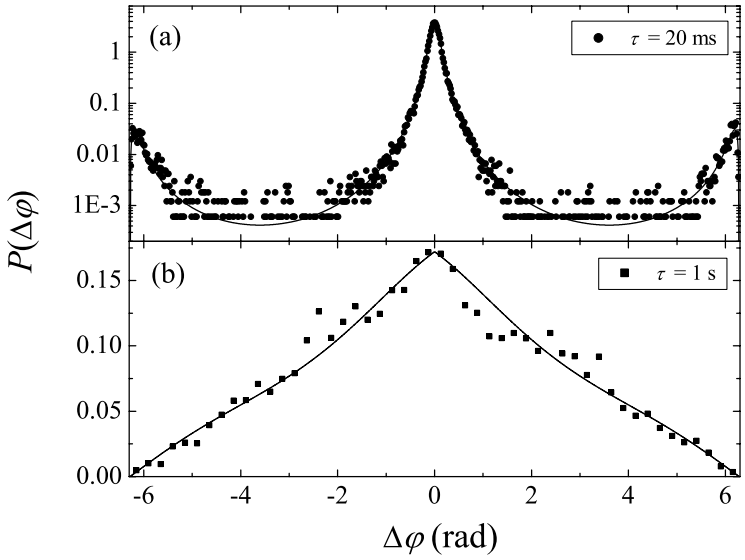

Figure 9. The wrapped phase difference probability distribution for two different time intervals τ. The solid symbols represent the experimental data, and the curves are the single-parameter fits of Eq. (12).

shows the algebraic form predicted by Eq. (13), but rises again near $\pm 2\pi$ due to the effect of the 2π jumps in the phase due to phase wrapping. At the longer time of $\tau = 1$ s, the shape of $P(\Delta\varphi)$ has changed completely and is starting to approach the triangular function predicted by Eq. (14). Thus, excellent agreement between theory and experiment is found over many orders of magnitude in $P(\Delta\varphi)$ and over the entire range of $\Delta\varphi$ from -2π to 2π, providing a very convincing demonstration of the validity of this theoretical model for the phase difference statistics.

Our theory for $P(\Delta\varphi)$ also provides a framework for using phase fluctuations of multiply scattered waves to measure the dynamics of complex media, thereby showing how phase information can be used in a regime where more traditional methods such as Doppler imaging break down. The relative mean square displacement of the scattering particles determined from fitting the full theory for $P(\Delta\varphi)$ (Eq. (12)) to our phase data is plotted as open symbols in Fig. 10 for a range of different times τ. In this figure, the results from the phase measurements are also compared with data obtained from the field correlation function, measured as described in section 2. Again excellent agreement is found, further confirming the validity of our model for the phase difference probability distribution. Thus, we can

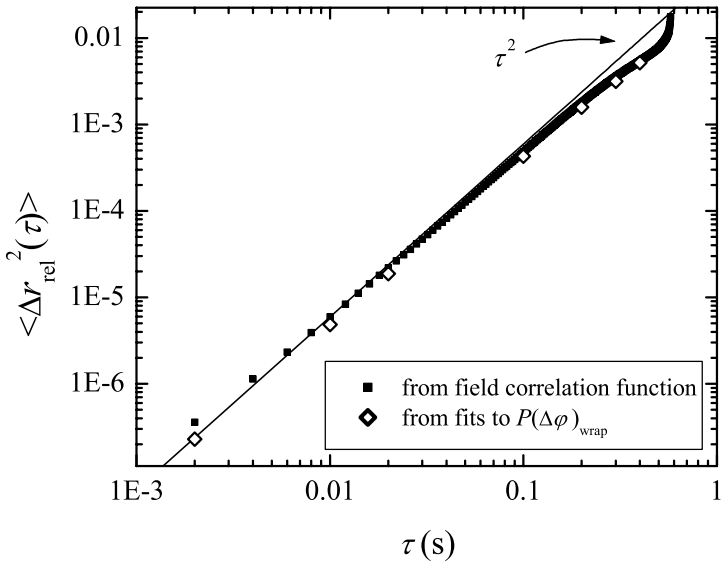

Figure 10. The mean square relative displacement of particles in a fluidized suspension measured from the width of the wrapped phase difference probability distribution (open diamonds) and directly from the field autocorrelation function (solid squares).

conclude that this investigation of the phase statistics of multiply scattered ultrasonic waves provides both a beautiful example of a novel mesoscopic wave phenomenon and an alternative approach for measuring the dynamic behaviour of multiply scattering systems.

3.2. AMPLITUDE INFORMATION: THE SIEGERT RELATION FOR MULTIPLY SCATTERED WAVES

By measuring simultaneously the fluctuations in the scattered amplitude and field, we are able to investigate the relationship between the intensity and field autocorrelation functions, and hence probe the range of validity of the Siegert relation for multiply scattered waves. The Siegert relation gives a simple link between these two correlation functions, and is often used in optics, especially for multiply scattered waves, to relate measurements of the intensity correlation function to theory for g_1 (e.g. see [26, 27, 28, 29]). Since the scattered intensity $I(T) \propto |A(T)|^2$, we can determine the intensity correlation function $G_2(\tau)$ directly from our measurements of amplitude

fluctuations, where

$$G_2(\tau) = \frac{\langle I(T)I(T+\tau)\rangle}{\langle I(T)\rangle^2} = 1 + \beta g_2(\tau). \tag{15}$$

Here β is the coherence factor, which is determined by the detector geometry and is normally close to unity. For complex random Gaussian fields, the correlation function $g_2(\tau)$ is equal to the square of the field correlation function $g_1(\tau)$, as expressed by the Siegert relation:

$$g_2(\tau) = |g_1(\tau)|^2 \tag{16}$$

Since we have shown above that the scattered wave field can be represented as a complex Gaussian random variable under the conditions for which the phase measurements were performed, it would seem natural to assume that this is always the case, and that the Siegert relation is generally obeyed for multiply scattered waves. In this section we study this question critically by examining the validity of the Siegert relation as a function of the path length of multiply scattered waves in fluidized suspensions, where the motions of the scatterers are at least locally correlated.

Pulsed DAWS measurements of the correlation functions $g_2(\tau)$ and $g_1(\tau)$ are shown in Fig. 11 for the same fluidized suspensions (glass beads in a water/gycerol mixture) used as examples of dynamic strongly scattering media throughout this paper. To ensure very efficient data collection, the amplitude of the scattered field was measured using a diode detector, and the field and amplitude sampled at the same point t_s in the scattered wave form using two separate boxcars. (The gate width in the boxcars was set to be much less than the wave period to enable the field to be accurately captured at a single point in the wave form.) Figure 11 shows that $g_2(\tau)$ and $|g_1(\tau)|^2$ are indistinguishable for long paths. However, for $n < 10$, $g_2(\tau)$ is significantly larger than $|g_1(\tau)|^2$ at all times τ, indicating clearly that the Siegert relation breaks down for short paths in this system. We have investigated this effect for different volume fractions of scatterers ranging from 0.245 to 0.5, and find similar behaviour at all volume fractions. To gain insight into this phenomenon, we compare the volume Ω_ξ over which the particle motions are correlated with the volume Ω_D probed by diffusing acoustic waves for 10 scattering events. From our DAWS and DSS measurements of the velocity correlation length ξ in the suspensions, we find that the particle correlation volume Ω_ξ ranges from about 500 mm^3 at $\phi = 0.245$ to 5000 mm^3 at $\phi = 0.5$. By contrast, simple estimates of Ω_D for $n = 10$ scattering events using the diffusion approximation are much smaller, ranging form 130 mm^3 at $\phi = 0.245$ to 17 mm^3 at $\phi = 0.5$. Thus, the motion of the particles in a path containing 10 steps is strongly correlated, leading to

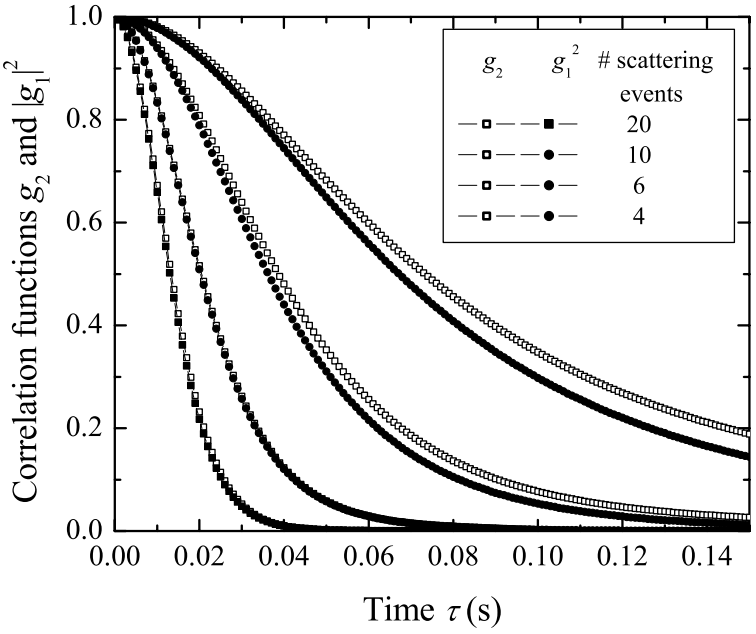

Figure 11. Comparison of the intensity (open symbols) and field (closed symbols) autocorrelation functions measured using pulsed DAWS for different path lengths of diffusing sound. The number of scattering events for each data set is shown in the insert.

the breakdown of the Siegert relation for short paths where the product of four fields in the intensity correlation function is coupled due to the relative motion. What is potentially of greater interest is the observation that for $n \geq 10$, even though the motion of the particles is still correlated in the volume explored by the multiply scattered waves, 10 or more scatterings are sufficient to overcome the effects of these correlations, thereby randomizing the cumulative phases of multiply scattered waves along different scattering paths so that the Siegert relation becomes valid. This conclusion also has important ramifications for continuous wave (cw) measurements, which correspond to the usual experimental situation in optical experiments such as DWS [26, 27, 28]. Since the average path length of cw waves in multiply scattering media is generally sufficiently large that the contributions for short paths containing fewer than 10 scattering events are negligible, the Siegert relation is expected to be valid whether or not there are correlations in systems' dynamics. We have verified this result through additional measurements of the field and intensity correlation functions for cw DAWS

in the same fluidized suspensions.

3.3. CONCLUSIONS

Diffusing Acoustic Wave Spectroscopy (DAWS) is a powerful approach for investigating the dynamics of strongly scattering media where direct imaging fails. Because the wavelengths of seismic waves, sound and ultrasound are very much larger that light, this technique and its many potential extensions are applicable to different classes of materials and systems than those that can be studied with the optical technique of DWS. DAWS is based on measurements of the scattered wave field, not intensity, so that it is an example of field fluctuation spectroscopy. This has important consequences not only for investigating the dynamics of complex media but also for studying wave phenomena in the presence of strong multiple scattering. Two examples of the latter have been presented in this paper: understanding the phase statistics of temporally fluctuating multiply scattered fields, and investigating the breakdown of the Siegert relation for multiply scattered waves due to particle velocity correlations.

In this paper, the potential applications of DAWS have been illustrated with experiments on fluidized suspensions of non-Brownian particles. In this case, DAWS provides a very sensitive probe of the local relative velocity of the particles as well as the correlations in the velocities over a wide range of length and time scales. Recently a number of other applications and analogous techniques have been or are being developed, including the monitoring of fish in a reverberant aquarium [30], the sensitive measurement of ultrasonic velocity changes with temperature [31] and the monitoring seismic and laboratory-scale events in geophysics, where the relevance of wave diffusion has recently been convincingly demonstrated[32] and field fluctuation spectroscopy with multiply scattering acoustic waves has been given the seismically relevant name of Coda Wave Interferometry [33]. Many other applications in the nondestructive evaluation of complex media will likely emerge in the future.

4. Acknowledgements

Support from Natural Sciences and Engineering Research Council of Canada is gratefully acknowledged.

5. References

References

1. Author to whom correspondence should be addressed. Email: jhpage@cc.umanitoba . ca Website: www.physics.umanitoba.ca/∼jhpage

2. Present address: Dept. of Physics, University of Toronto, 60 St. George St., Toronto, Ontario M5S 1A7 Canada
3. *Scattering and Localization of Classical Waves in Random Media*, edited by P. Sheng (World Scientific, Singapore, 1990).
4. P. Sheng, *Introduction to Wave Scattering, Localization, and Mesoscopic Phenomena*, (Academic Press, San Diego, 1995).
5. *Diffuse Waves in Complex Media*, edited by J.-P. Fouque, (Kluwer, Dordrecht, 1999)
6. *Photonic Crystals and Light Localization in the 21st Century*, edited by C. M. Soukoulis, (Kluwer, Dordrecht, 2001)
7. M. L. Cowan, J. H. Page and D. A. Weitz, *Phys. Rev. Lett.* **85**, 453 (2000).
8. J. H. Page, M. L. Cowan and D. A. Weitz, *Physica B* **279**, 130 (2000).
9. J. H. Page, M. L. Cowan, P. Sheng and D. A. Weitz, in *IUTAM Symposium 99/4: Mechanical and Electromagnetic Waves in Structured Media*, edited by R. C. McPhedran, L. C. Botten and N. A. Nicorovici (Kluwer Academic, 2001), p. 121.
10. M. L. Cowan, I. P. Jones, J. H. Page, and D. A. Weitz, *Phys. Rev. E.* **65**, 066605 (2002).
11. D. Bicout and R. Maynard, *Physica A* **1993**, 387 (1993).
12. D. Bicout and G. Maret, *Physica A* **210**, 87 (1994).
13. M. L. Cowan, *Ph.D. Thesis* (University of Manitoba, 2001).
14. J. H. Page, H. P. Schriemer, A. E. Bailey and D. A. Weitz, *Phys. Rev. E* **52**, 3106 (1995).
15. J. H. Page, P. Sheng, H. P. Schriemer, I. Jones, X. Jing and D. A. Weitz, *Science* **271**, 634 (1996).
16. H. P. Schriemer, M. L. Cowan, J. H. Page, P. Sheng, Z. Liu, and D. A. Weitz, it Phys. Rev. Lett. **79**, 3166 (1997).
17. A. Tourin, A. Derode, P. Roux, B. A. van Tiggelen and M. Fink, *Phys. Rev. Lett.* **79**, 3637 (1997).
18. M. L. Cowan, K. Beaty, J. H. Page, Z. Liu and P. Sheng, *Phys. Rev. E* **58**, 6626 (1998).
19. P. N. Segrè, E. Herbolzheimer and P. M. Chaikin, *Phys. Rev. Lett.* **79**, 2574 (1997).
20. M. P. Brenner, it Phys. Fluids **11**, 754 (1999).
21. D. L. Koch and E. S. G. Shaqfeh, *J. Fluid Mech.* bf 224, 275 (1991).
22. A. Levine, S. Ramaswamy, E. Frey, and R. Bruinsma, *Phys. Rev. Lett.* **81**, 5944 (1998).
23. J. W. Goodman, *Statistical Optics* (Wiley, New York, 1985).
24. B. A. van Tiggelen, P.Sebbah, M. Stoytchev, and A. Z. Genack, *Phys. Rev. E* **59**, 7166 (1999).
25. A. Z. Genack, P.Sebbah, M. Stoytchev, and B. A. van Tiggelen, *Phys. Rev. Lett.* **82**, 715 (1999).
26. G. Maret and P. E. Wolf, *Z. Phys. B* **65**, 409 (1987).
27. D. J. Pine, D. A. Weitz, P. M. Chaikin and E. Herbolzheimer, *Phys. Rev. Lett.* **60**, 1134 (1988).
28. D. J. Pine, D. A. Weitz, G. Maret, P. E. Wolf, E. Herbolzheimer, and P. M. Chaikin, in *Scattering and Localization of Classical Waves in Random Media*, edited by P. Sheng (World Scientific, Singapore, 1990) p. 312.
29. J. X. Zhu, D. J. Pine and D. A. Weitz, *Phys. Rev. A* **44**, 3948 (1991).
30. J. de Rosny and P. Roux, it J. Acoust. Soc. Am. **109**, 2587 (2001).
31. R. L. Weaver and O. I. Lobkis, *Ultrasonics* **38**, 491 (2000).
32. M. Campillo, L. Margerin and Nikolao Shapiro, in *Diffuse Waves in Complex Media*, edited by J.-P. Fouque, (Kluwer, Dordrecht, 1999) p. 383.
33. R. Snieder, A. Gret, H. Douma, and J. Scales, *Science* **295**, 2253, (2002).